Tailored TiO_2—$SrTiO_3$ Heterostructure Nanotube Arrays for Improved Photoelectrochemical Performance

Jun Zhang,[†,‡] Jin Ho Bang,[†] Cencun Tang,[§] and Prashant V. Kamat[†,*]

[†]Radiation Laboratory and Department of Chemistry and Biochemistry, University of Notre Dame, Notre Dame, Indiana 46556, [‡]College of Physical Science and Technology, Central China Normal University, Wuhan 430079, China, and [§]School of Material Science and Engineering, Hebei University of Technology, Tianjin 300130, China

ABSTRACT TiO_2 nanotube arrays formed on Ti substrate by electrochemical anodization have been converted into TiO_2—$SrTiO_3$ heterostructures by controlled substitution of Sr under hydrothermal conditions. The growth of $SrTiO_3$ crystallites on the nanotube array electrode was probed by electron microscopy and X-ray diffraction. As the degree of Sr substitution increases with the duration of hydrothermal treatment, an increase in the size of $SrTiO_3$ crystallites was observed. Consequently, with increasing $SrTiO_3$ fraction in the TiO_2—$SrTiO_3$ nanotube arrays, we observed a shift in the flat band potential to more negative potentials, thus confirming the influence of $SrTiO_3$ in the modification of the photoelectrochemical properties. The TiO_2—$SrTiO_3$ composite heterostructures obtained with 1 h or less hydrothermal treatment exhibit the best photoelectrochemical performance with nearly 100% increase in external quantum efficiency at 360 nm. The results presented here provide a convenient way to tailor the photoelectrochemical properties of TiO_2—$SrTiO_3$ nanotube array electrodes and employ them for dye- or quantum-dot-sensitized solar cells and/or photocatalytic hydrogen production.

KEYWORDS: TiO_2—$SrTiO_3$ nanotube arrays · nanocomposites · photoelectrochemistry · heterostructure · hydrothermal reaction

Design and development of nanostructure semiconductor assemblies has drawn significant interest in recent years because of their application in the development of economically viable solar cells and photocatalytic systems.[1−5] Of particular interest are one-dimensional (1-D) architectures, such as TiO_2 nanotube arrays, which serve as a scaffold to anchor light-harvesting assemblies. For example, TiO_2 nanotube arrays have been successfully employed in dye- and quantum-dot-sensitized solar cells.[6−12] In addition, they have been found to be useful as a photoanode in water-splitting reaction.[13−16] Such one-dimensional architectures facilitate transport of charge carriers with greater efficiency than mesoscopic or particulate semiconductor films and thus minimize the loss of charge carriers at grain boundaries.[7−9,17] Significant improvement in the photoconversion efficiencies has been reported using such 1-D TiO_2 nanotube and carbon nanotube arrays in solar cells.[4,8−10,18−25]

TiO_2 responds only in the UV region because of its large band gap.[26] The TiO_2 nanotube arrays when employed as a photoanode in a photoelectrochemical cell exhibit relatively low photoconversion efficiency; for example, TiO_2 nanotubes prepared by electrochemical etching can split water only under external bias.[16,27] To improve the photoconversion efficiency, TiO_2 was coupled with semiconductors such as SnO_2, CdS, and CdSe to facilitate charge separation.[28−38] In other strategies to boost up the efficiency, TiO_2 was often doped with light elements (*e.g.*, C or N) to harvest visible light.[39−43] Another approach is to develop ternary oxides (ABO_3) such as perovskites on TiO_2 surfaces through exchange of cations by wet-chemical synthesis.[44−47] These ternary metal oxides have been found to be catalytically active, and their application in storage batteries and photocatalysis has been explored by several researchers.[48−51] $SrTiO_3$ offers favorable energetics for photocatalysis since its conduction band edge is 200 mV more negative than TiO_2.[52] This makes $SrTiO_3$ a good candidate for coupling TiO_2 and improving photoelectrochemical performance by shifting the Fermi level of the composite to more negative potentials.

Recently, *n*-Si/*n*-TiO_2 core/shell nanowire arrays and TiO_2/$TiSi_2$ heterostructures have been reported for highly efficient photoelectrochemical cells.[53,54] Both these newly developed systems, however, suffer from poor photostability in water and positive shifts of their apparent Fermi level. Given the stability of TiO_2 and $SrTiO_3$, it is of interest to see whether one can develop a TiO_2—$SrTiO_3$ heterostructure in a controlled way. Coupling $SrTiO_3$ to TiO_2 can provide synergies for achieving better charge separation and thus producing improved

*Address correspondence to pkamat@nd.edu.

Received for review August 25, 2009 and accepted December 1, 2009.

Published online December 15, 2009.
10.1021/nn901087c

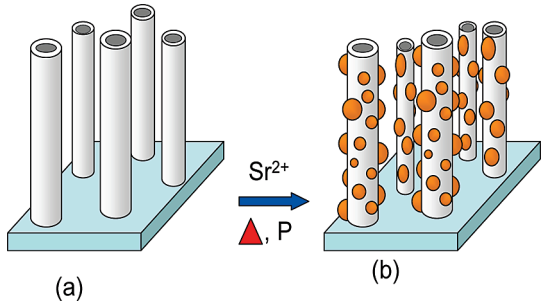

Scheme 1. Synthetic approach for designing TiO_2−$SrTiO_3$ heterostructure.

photocurrent and photovoltage in a photoelectrochemical cell. Controlled substitution of Sr into TiO_2 nanotube arrays has provided us with a means to examine the influence of $SrTiO_3$ in improving the photoelectrochemical performance of a heterostructured photocatalyst (Scheme 1). The synthesis and characterization of TiO_2−$SrTiO_3$ nanotube arrays and their photocurrent response to UV excitation are discussed.

RESULTS AND DISCUSSION

Formation of $SrTiO_3$ Nanocrystallites on TiO_2 Nanotube Scaffolds. Electrochemical anodization of Ti foil in a fluoride medium produces an ordered array of TiO_2 nanotubes.[55−60] Upon annealing at 450 °C in air, these arrays form anatase crystallites while maintaining the tubular morphology. The SEM image in Figure 1a shows the TiO_2 nanotube arrays prepared by this procedure. The resulting TiO_2 nanotube arrays consist of uniform size tubes of an average length of 1.5 μm and a diameter of 70 nm. The bundling of these tubes at the tips is caused by capillary stress during the evaporation of solvent during drying. Solvent surface tension plays an important role in minimizing the bending of these nanotubes during the annealing process.[61] The inset in Figure 1a shows a TEM image of a single TiO_2 nanotube obtained after sonication of the TiO_2 film in water. The nanotube, which has a wall thickness of 15 nm, consists of aggregated particles. This aggregation seen in the TiO_2 nanotubes has been systematically investi-

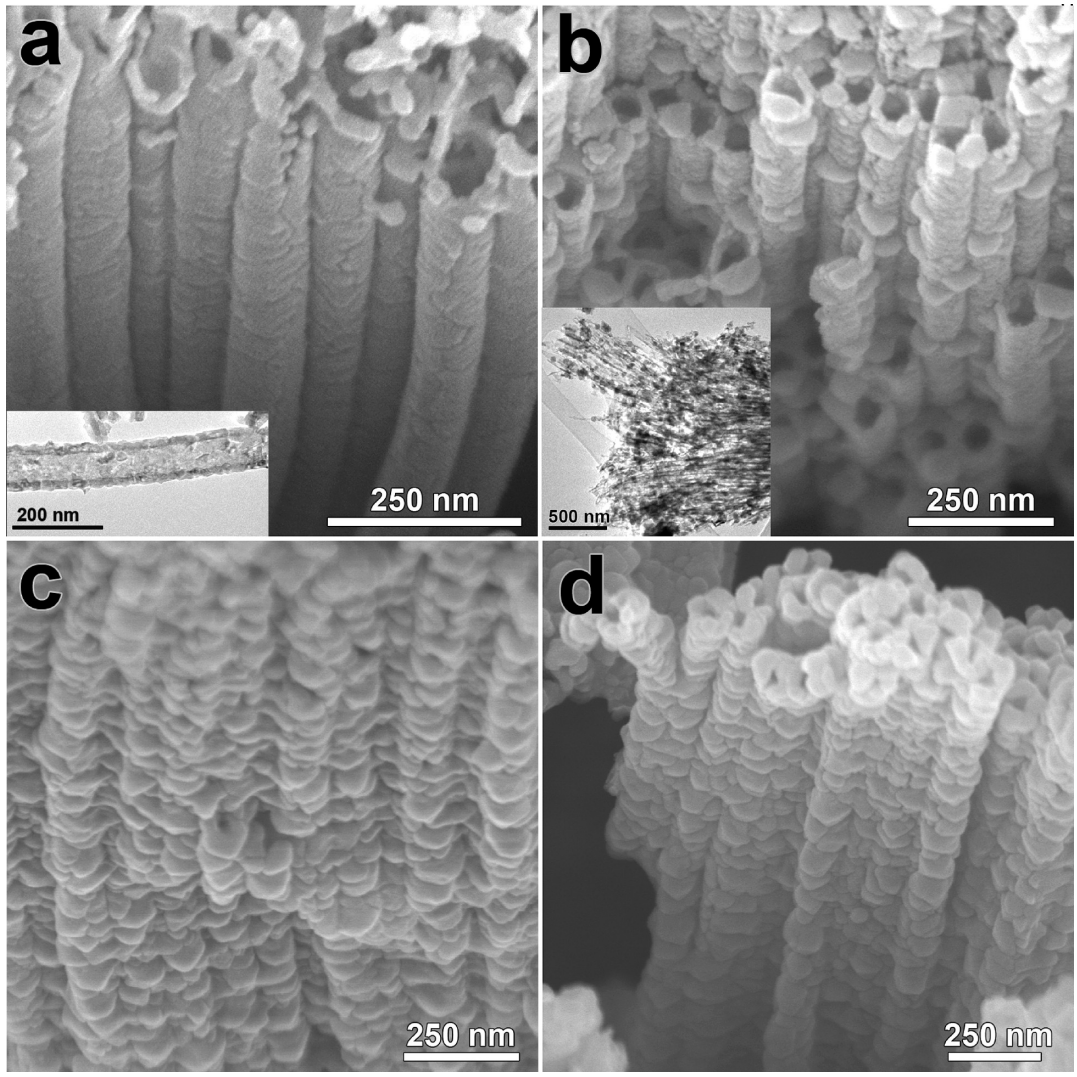

Figure 1. SEM images of four different electrodes: (a) TiO_2 nanotube array after annealing at 450 °C and TEM image of a single nanotube (inset); (b) TiO_2−$SrTiO_3$ nanocomposite obtained after 1 h hydrothermal treatment and TEM image of the corresponding nanotubes (inset); (c) TiO_2−$SrTiO_3$ nanocomposites obtained after 2 h and (d) 40 h hydrothermal reaction.

gated in a previous work.[62] Tubular structure, with nearly uniform pore diameter of 70 nm throughout the length of the tube, is consistent with our SEM observation. XRD pattern of the annealed TiO_2 (bottom trace in Figure 2) confirms the formation of anatase phase during the heat treatment of TiO_2 nanotube array. (Note that the Ti peaks stem from the titanium substrate and are also detected in all other samples.)

$SrTiO_3$ nanoparticle-coated TiO_2 nanotube arrays were prepared by utilizing the preformed anatase nanotube arrays as a TiO_2 source as well as a structure-directing scaffold. In our synthesis, the amount of $SrTiO_3$ coating was readily tuned by varying hydrothermal reaction times and, as will be discussed in a later section, it turned out that the degree of coverage of $SrTiO_3$ over TiO_2 is a key parameter governing the photoelectrochemical properties of the heterostructure nanocomposites.

We systematically examined the composition of TiO_2 nanotube arrays obtained after hydrothermal treatment in water containing Sr^{2+} at different time intervals. The sample drawn after 0.5 h hydrothermal treatment mainly exhibited XRD peaks corresponding to anatase TiO_2 and Ti substrate. No peaks corresponding to $SrTiO_3$ could be detected. TEM images did not show any significant change in the morphology. At reaction time equal to 1 h, changes in the TiO_2 nanotube arrays were apparent. An SEM image of the sample after hydrothermal reaction time of 1 h is shown in Figure 1b. Nanoparticles with a diameter of ~50 nm are formed on the surface of TiO_2 nanotubes. Appearance of these small crystallites shows the morphological changes associated with Sr substitution during hydrothermal treatment. The formation of $SrTiO_3$ in basic solution is known to proceed through a titanate intermediate, which facilitates substitution of a cation with Sr^{2+}.[63] Although such a substitution process is likely to start from the beginning, we first start noticing these changes at 1 h. The distribution of the nanoparticles over the nanotubes indicates preferential nucleation and growth of the nanoparticles on defect sites on the TiO_2 surfaces. Additional confirmation for the exchange of Sr^{2+} ions was also obtained from XPS analysis. The XPS spectra of 0.5 and 1 h treated samples are shown in the Supporting Information (Figure S1).

The particle growth process continues as we extend the hydrothermal treatment up to 40 h. Panels c and d of Figure 1 show the TEM images of samples after 2 and 40 h, respectively. It is evident from the TEM observation that the nanoparticles are mostly formed on the outer surface of TiO_2 nanotubes. Such a morphological feature implies that the formation of the nanoparticles is governed by the diffusion of Sr^{2+} ions from solution to the outer surface of nanotubes. The evolution of the TiO_2—$SrTiO_3$ composite structure can be seen from the XRD pattern recorded with samples drawn at different hydrothermal treatment times (Figure 2). The peaks corresponding to both $SrTiO_3$ and TiO_2 are seen in samples with 1 h or greater duration of hydrothermal treatment. The increase in peak intensity relative to TiO_2 with increasing time shows that the formation of $SrTiO_3$ continues to maximize the Sr^{2+} exchange and form $SrTiO_3$ nanocrystallites on the TiO_2 nanotemplate. Even after 40 h of hydrothermal treatment, we are able to maintain a robust heterostructure consisting of $SrTiO_3$ nanocrystallites with TiO_2 nanotube scaffold. Such vertically aligned heterostructure nanotube arrays are likely to have a wide range of applications in the development of semiconductor-based photocatalysts.

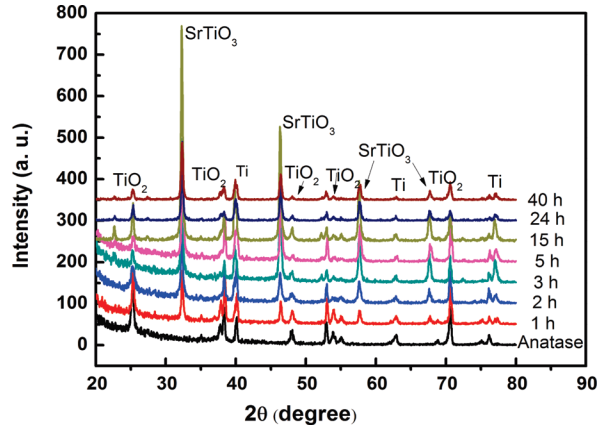

Figure 2. XRD patterns of TiO_2 nanotube array after annealing and TiO_2—$SrTiO_3$ nanocomposites obtained after hydrothermal treatment for different durations. Ti peaks originate from Ti metal substrate.

Further evidence for the formation of $SrTiO_3$ nanocrystallites on the outer surface of TiO_2 nanotubes was confirmed by STEM-EDS (Figure 3). The line analysis over the span of 796 nm of nanocomposite reveals a distinct signal corresponding to the Sr element in the region of the small nanocrystallites. The space between the nanocrystallites is dominated by the Ti elemental signal corresponding to the presence of TiO_2. The broad signal arising from O represents both $SrTiO_3$ and TiO_2. The XRD and TEM analyses thus confirm the decoration of TiO_2 nanotube arrays with $SrTiO_3$ nanocrystallites.

Importance of TiO_2 Crystallinity in Controlling Morphology of the Heterostructures. It is interesting to note that the TiO_2—$SrTiO_3$ heterostructure films discussed above were obtained from annealed nanocrystalline TiO_2 nanotube arrays. The existence of TiO_2 crystal phase

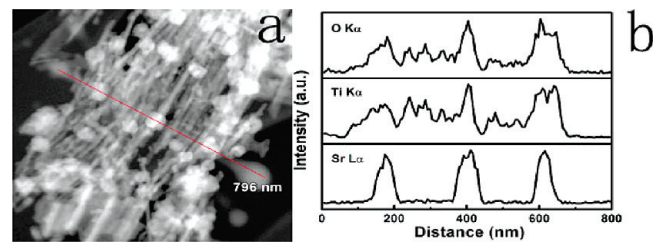

Figure 3. (a) STEM image of the TiO_2—$SrTiO_3$ nanocomposite obtained after 1 h hydrothermal treatment and (b) corresponding EDS line analysis.

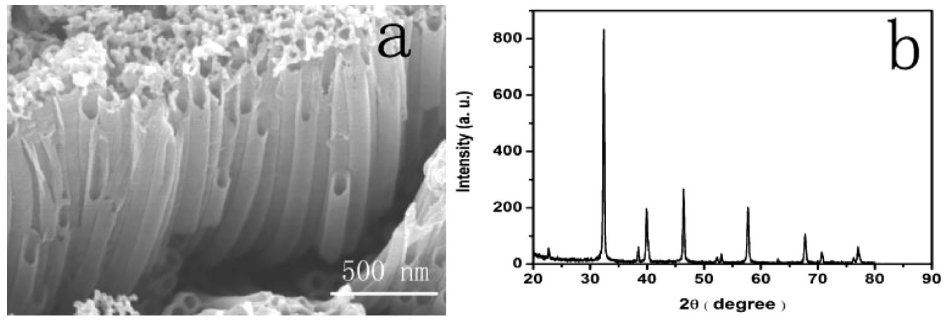

Figure 4. (a) SEM and (b) XRD of $SrTiO_3$ nanotubes obtained following 2 h hydrothermal treatment of amorphous TiO_2 nanotube arrays.

even at long-time-treated samples supports our claim that the $SrTiO_3$ is formed as separate nanocrystallites on the TiO_2 nanotubes, and their formation is controlled by the penetration rate of Sr^{2+} ions. As $SrTiO_3$ crystallites grow with the duration of hydrothermal treatment, the outer layer retards the penetration of Sr^{2+} ions into the TiO_2 nanotubes and thus slows down the exchange process. In contrast, if we employ unannealed TiO_2 nanotubes, their amorphous character provides facile substitution of Sr. Figure 4a shows the SEM image of the sample obtained after 2 h hydrothermal treatment of unannealed TiO_2 nanotube arrays. The samples were transferred to the autoclave after electrochemical etching of Ti film. The morphology of these tubes remains undisturbed, while the XRD pattern (Figure 4b) confirms the formation of $SrTiO_3$. Although the TiO_2 nanotubes were amorphous, we were able to obtain $SrTiO_3$ nanotubes in the crystalline form while maintaining the vertical alignment of the nanotube array. Our observation in the reaction of $Sr(OH)_2$ with amorphous TiO_2 nanotubes is consistent with the previous reports.[64−67] However, the pure $SrTiO_3$ nanotube arrays obtained from amorphous TiO_2 films were inferior for the generation of photocurrent during the evaluation of photoelectrochemical behavior (see Supporting Information Figure S2). Hence, the following discussion on the photoelectrochemical properties will involve films shown in Figures 1 and 2.

Photoelectrochemistry. The semiconducting nature of the TiO_2−$SrTiO_3$ heterostructure makes it suitable for the development of photoelectrochemical cells and photocatalysts. As shown earlier,[7−11] TiO_2 nanotube arrays act as an excellent support to anchor light-harvesting assemblies, such as dyes and semiconductor nanocrystals. Similarly, TiO_2 nanotube arrays have also been employed in photocatalytic water-splitting process.[4] In order to evaluate the properties of the TiO_2−$SrTiO_3$ heterostructure arrays (samples shown in Figures 1 and 2), we employed them as photoanodes in a 3-arm photoelectrochemical cell. A Pt counter electrode and 0.1 M NaOH as electrolyte were employed, and the TiO_2−$SrTiO_3$ electrodes were illuminated with UV−visible light ($\lambda > 300$ nm).

The photocurrent responses of TiO_2 and TiO_2−$SrTiO_3$ electrodes prepared with different hydrothermal reaction times are shown in Figure 5. The photocurrent response to illumination was prompt in all cases, but the magnitude of photocurrent varied depending upon the extent of hydrothermal treatment. The TiO_2 nanotube electrodes subjected to 1 h or less hydrothermal treatment exhibited greater photocurrent than the untreated TiO_2 nanotube electrode. As a control experiment, TiO_2 nanotubes were hydrothermally treated under the same condition without $Sr(OH)_2$, and it was revealed that no structural change occurred even after the treatment, and moreover, the photoelectrochemical response was identical, confirming that the improvement in photocurrent solely stems from coupling TiO_2 with $SrTiO_3$.

With longer treatment times, the photocurrent decreased. Note, while the electrode obtained after 0.5 h treatment initially yielded higher photocurrent, it was unable to be sustained during short-term continuous illumination. The reason for the gradual decrease in activity is still unknown and under investigation, but the instability of photocurrent in the 0.5 h treated electrode is likely to arise from the weaker stability and crystallinity of $SrTiO_3$ nuclei, as recognized from XRD and XPS analysis. However, the TiO_2−$SrTiO_3$ heterostructure obtained after 1 h hydrothermal treatment provides a stable photocurrent and hence is considered to be superior to other electrodes.

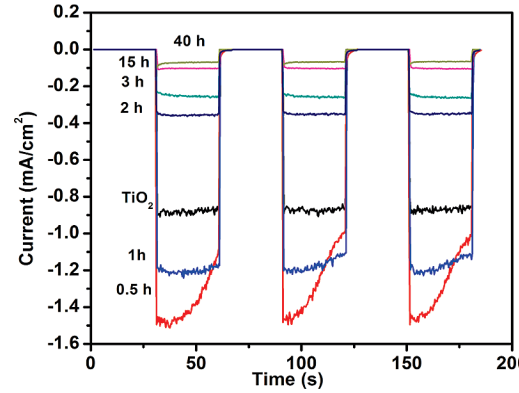

Figure 5. Current *versus* time measurements of TiO_2 nanotube and TiO_2−$SrTiO_3$ nanocomposite electrodes.

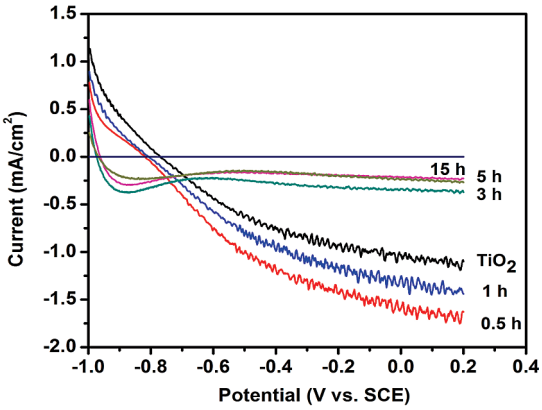

Figure 6. *I*−*V* characteristics of TiO_2 nanotube array electrode before and after hydrothermal treatment for varying times. The duration of treatment times varies the composition and structural aspects of TiO_2−$SrTiO_3$ heterostructure electrodes (electrolyte = 0.1 M NaOH, Pt counter electrode, and excitation = λ > 300 nm).

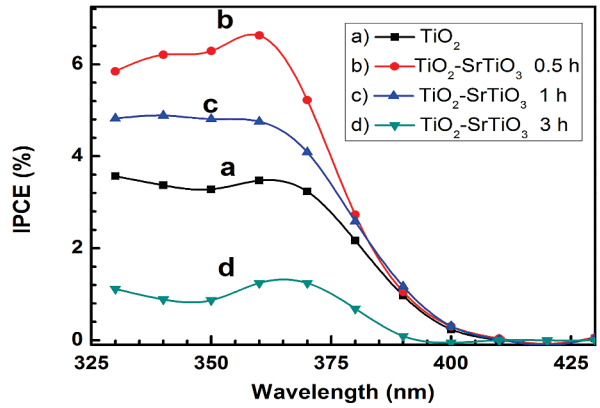

Figure 7. IPCE spectra of TiO_2 nanotube and TiO_2−$SrTiO_3$ nanocomposite electrodes recorded under no applied external bias.

We further evaluated the photoelectrochemical behavior of TiO_2 and TiO_2−$SrTiO_3$ electrodes by recording *I*−*V* characteristics (Figure 6). Untreated TiO_2 array electrode exhibits a zero current potential or flat band potential at −0.780 V *vs* SCE. A negative shift of ~50 mV is seen with TiO_2 nanotube array electrodes obtained during the initial times (≤1 h) of hydrothermal treatment. The shift is more significant for samples subjected to hydrothermal treatment greater than 1 h. For samples with 3−15 h treatment, this shift is as high as 200 mV. As discussed earlier,[32,68−70] the flat band potential represents the apparent Fermi level of a semiconductor in equilibrium with a redox couple. Since the Fermi level lies close to the conduction band of the n-type semiconductor, we expect the zero current potential to represent the effect of $SrTiO_3$ on the Fermi level of the TiO_2−$SrTiO_3$ heterostructure. While TiO_2 dominates the semiconductor properties of TiO_2−$SrTiO_3$ during early times (≤1 h), the small shift of 50 mV in the zero current potential shows that the Fermi level renders the composite more reductive. The shift in the Fermi level to negative potential is indicative of larger accumulation of electrons in the coupled heterostructure and reflects decreased recombination of charge carriers. These observations are consistent with our previous result of a TiO_2/Au nanocomposite in which deposition of Au nanoparticles achieves the Fermi level equilibration and suppresses charge recombination.[70] $SrTiO_3$ layer has also been proposed to induce dipole effects arising from the difference in electron affinity of two different semiconductors. For example, such dipole effect has been discussed by Zaban and co-workers to explain higher photovoltage seen in the sensitization of the TiO_2−$SrTiO_3$ composite.[44,71] We consider such dipole-induced effects to be minimal since we excite both semiconductors with UV light. The proposed shift in Fermi level in our experiments is mainly governed by charge separation within the heterostructure.

With longer hydrothermal treatment, the $SrTiO_3$ nanocrystallites grow to attain independent identity within the heterostructure. Since most of the excited light is adsorbed by $SrTiO_3$ nanocrystallites, we see a major shift of ~200 mV in the flat band potential. This shift in the flat band potential correlates well with the difference seen in the conduction band energies of TiO_2 and $SrTiO_3$ (E_{CB} (TiO_2) = −1.2 V *vs* SCE and E_{CB} ($SrTiO_3$) = −1.4 V *vs* SCE).[72,73]

The photoelectrochemical response of these electrodes to monochromatic light irradiation was evaluated in terms of incident photon to charge carrier efficiency (IPCE). The IPCE was determined from short circuit photocurrents monitored at different excitation wavelengths using the equation

$$\text{IPCE (\%)} = [1240/\lambda\ (\text{nm})][(I_{sc}\ (\text{A/cm}^2)/P_i\ (\text{W/cm}^2)] \times 100 \quad (1)$$

where P_i is the power of monochromatic light of wavelength λ (nm) incident on the electrode, and I_{sc} is short circuit current. The IPCE spectra of the TiO_2 nanotube array electrode, as well as 0.5, 1, and 3 h treated TiO_2−$SrTiO_3$ heterostructure electrodes (Figure 7), show an onset wavelength around 400 nm, suggesting that the band gap energy of these heterostructures remains unaltered. It may be noted that the band gaps of TiO_2 and $SrTiO_3$ are similar (E_g ~ 3.2 eV).[72] The absorption spectra recorded for these electrodes (see Supporting Information Figure S3) show similar absorption onset matching the IPCE characteristics. The maximum efficiencies of the 0.5 and 1 h treated nanocomposites obtained *under no applied external bias* were 6.7 and 4.8% as compared to 3.6% IPCE of the TiO_2 nanotube array electrode. Under applied external bias, the IPCE values increase significantly. Hence, caution should be exercised when comparing the efficiency values in the literature. The higher efficiency observed for the TiO_2−$SrTiO_3$ heterostructure array electrode shows im-

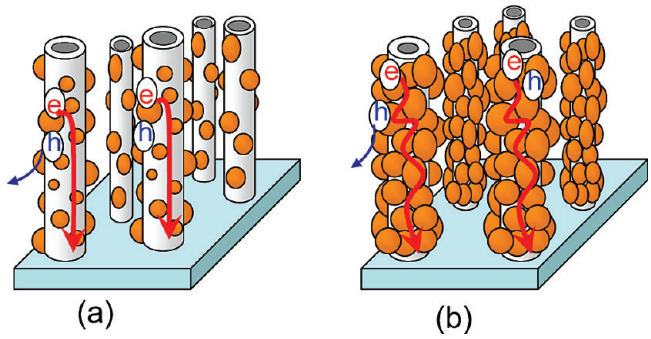

Scheme 2. Depiction of TiO_2−$SrTiO_3$ heterostructure (a) during early and (b) longer times of hydrothermal treatment of TiO_2 nanotube arrays.

proved charge separation and agrees with the results presented in Figures 6 and 7.

The results presented in Figures 5−7 show the importance of attaining a desired composition in the TiO_2−$SrTiO_3$ heterostructure so that the photoconversion efficiency can be maximized. The stable and efficient heterostructure arrays can be obtained with 1 h hydrothermal treatment of TiO_2 nanotube arrays in Sr^{2+} solution. The photocurrent responses of the TiO_2−$SrTiO_3$ heterostructure array electrode obtained from 2 h and longer hydrothermal treatment were lower than the untreated TiO_2 array electrode.

Scheme 2 illustrates two different types of morphologies that strongly influence the photoelectrochemical behavior of the TiO_2−$SrTiO_3$ heterostructure. The results shown in Figures 1 and 2 indicate that initial Sr substitution produces small, well-dispersed nuclei of $SrTiO_3$ on TiO_2 nanotubes during short duration hydrothermal treatment. Direct coupling of TiO_2 and $SrTiO_3$ nanostructures causes the Fermi level to equilibrate and reduce the recombination of charge carriers at the surface of the heterostructure. The vectorial electron transfer through aligned TiO_2 nanotubes promotes charge transport and thus improves the photoconversion efficiency. At longer hydrothermal times with the continuous substitution of Sr, the $SrTiO_3$ nuclei grow to become larger nanocrystallites. These closely packed $SrTiO_3$ nanocrystallites act more like an independent system with electron transport limited by their grain boundaries. The inner TiO_2 nanotube, being lost in its conversion to $SrTiO_3$, has little influence in transporting electrons. Although the performance of the $SrTiO_3$ nanocrystal array is rather poor, one can introduce additional measures to promote charge transport. For example, when 2 h hydrothermal-treated samples were annealed at 400 °C in air, they exhibited higher short circuit photocurrent (see Supporting Information Figure S4). Although the short circuit photocurrent nearly doubled after annealing, the overall photocurrent remained less than that of the untreated TiO_2 nanotube array electrode. In case of the 0.5 and 1 h treated nanocomposites, however, no significant improvement in photocurrent was observed even after the post-annealing.

CONCLUSIONS

The synthetic approach discussed here provides a facile way to achieve controlled growth of $SrTiO_3$ particles over TiO_2 nanotube arrays. The hydrothermal treatment promotes substitution of strontium in the TiO_2 nanotube array to yield a TiO_2−$SrTiO_3$ heterostructure with controlled morphology. The photoelectrochemical performance of such a vertically aligned heterostructure array is strongly dependent on its composition and morphology. Only well-dispersed $SrTiO_3$ nanocrystallites on TiO_2 nanotube arrays improved the overall photoelectrochemical performance. Currently, efforts are underway to utilize these heterostructured nanocomposites in the application of quantum-dot-sensitized solar cells, and our preliminary investigation shows further usefulness of the nanocomposites for better solar cell performance.

EXPERIMENTAL METHODS

Synthesis of TiO_2 Nanotube Arrays on Ti Substrate. Titanium foil (0.25 mm in thickness, >98% from Aldrich) was cut into 0.8 cm × 2.5 cm strips. These strips were degreased by sonication in isopropanol for 1 h after which they were stored in acetone. The titanium foil was placed in an electrochemical cell equipped with a platinum mesh counter electrode and a power supply. Ammonium fluoride (0.3 wt %) in ethylene glycol (2 v/v % in water) was used as an electrolyte. A constant potential of 55 V was applied at a rate of 1 V/s between the two electrodes for 1.5 h. After the reaction, the strip was removed from the cell and washed with deionized water. A 1−5 s sonication was performed to remove any surface deposits. The films were then annealed at 450 °C in dry air for 3 h with a temperature ramp rate of 1 °C min^{-1} at both the processes of warm up and cool down.

Synthesis of TiO_2−$SrTiO_3$ Heterostructure Nanotube Arrays. The annealed TiO_2 nanotube array films produced by the above procedure were utilized as a TiO_2 source for the fabrication of $SrTiO_3$. The TiO_2 nanotube arrays also acted as a structure-directed template for the formation of the TiO_2−$SrTiO_3$ heterostructure. In a typical experiment, 0.565 g of strontium hydroxide octahydrate, $Sr(OH)_2 \cdot 8H_2O$, was added to 85 mL of deionized water while stirring at room temperature. Once fully dissolved, the resulting solution was transferred to a Teflon-lined stainless steel autoclave, filling 80% of the total volume. A piece of a TiO_2 nanotube array stripe was then immersed in the solution. The autoclave was sealed and placed in an oven at 180 °C for different reaction times. After the hydrothermal reaction, the autoclave was taken out and cooled down by flowing tap water. The strip was washed with deionized water and ethanol several times and then dried under air flow for characterization and photoelectrochemical measurements.

Characterization. The composition and crystal structure of the obtained films were examined by an X-ray diffractometer (Scintag X1 advanced diffraction system). The sample morphology was observed using a field-emission scanning electron microscope (Hitachi S-4800 FESEM). Transmission electron microscopy (TEM) and scanning transmission electron microscopy (STEM) were carried out using a JEOL 2010F equipped with EDS (energy-dispersive

X-ray spectroscopy) detector at an acceleration voltage of 200 kV. X-ray photoelectron spectroscopy (XPS) measurements were conducted by a Kratos axis ultra imaging X-ray photoelectron spectrometer. Diffuse reflectance UV−vis adsorption spectra were recorded using a Shimadzu UV-3101 PC spectrophotometer; Ti foil preheated at 450 °C under air was used as a reference.

Photoelectrochemical Measurements. The TiO_2 nanotube arrays and TiO_2−$SrTiO_3$ heterostructured nanotubes were employed as photoanodes in a 3-arm cell. The top of the electrodes were mechanically polished for electrical contact. Current−voltage (I−V) characteristics were recorded using a Princeton Applied Research potentiostat PARSTAT 2263 in a three-electrode configuration using Pt gauze as a counter electrode, a saturated calomel electrode (SCE) as a reference, and 0.1 M NaOH solution as an electrolyte. Photocurrent measurements were carried out in a two-electrode configuration using a Keithley 617 programmable electrometer along with collimated, filtered light ($CuSO_4$ filter, $\lambda > 300$ nm) from an Oriel 450 W xenon arc lamp. A Bausch and Lomb high-intensity grating monochromator was introduced into the path of the excitation beam for selecting a wavelength during incident photon to charge carrier efficiency (IPCE) measurement. All experiments were carried out under ambient conditions.

Acknowledgment. We gratefully acknowledge Prof. K. S. Suslick for his generous permission to use his facilities. J.Z. thanks the China Scholarships Council for the research grant. This research was carried out, in part, at the Center for Microanalysis of Materials, UIUC, which is partially supported by the U.S. Department of Energy under Grant DE-FG02-07ER46418. The research described herein was supported by the Department of Energy, Office of Basic Energy Sciences. This is contribution number NDRL-4812 from the Notre Dame Radiation Laboratory.

Supporting Information Available: XPS spectra, photocurrent response of pure $SrTiO_3$ nanotube arrays, diffuse reflectance absorption spectra, and comparison of photocurrent of TiO_2−$SrTiO_3$ electrodes (2 h) before and after heat treatment are presented. This material is available free of charge *via* the Internet at http://pubs.acs.org.

REFERENCES AND NOTES

1. Kamat, P. V. Meeting the Clean Energy Demand: Nanostructure Architectures for Solar Energy Conversion. *J. Phys. Chem. C* **2007**, *111*, 2834–2860.
2. Lewis, N. S.; Nocera, D. G. Powering the Planet: Chemical Challenges in Solar Energy Utilization. *Proc. Natl. Acad. Sci. U.S.A.* **2006**, *103*, 15729–15735.
3. Maeda, K.; Domen, K. New Non-Oxide Photocatalysts Designed for Overall Water Splitting under Visible Light. *J. Phys. Chem. C* **2007**, *111*, 7851–7861.
4. Shankar, K.; Basham, J. I.; Allam, N. K.; Varghese, O. K.; Mor, G. K.; Feng, X.; Paulose, M.; Seabold, J. A.; Choi, K.-S.; Grimes, C. A. Recent Advances in the Use of TiO_2 Nanotube and Nanowire Arrays for Oxidative Photoelectrochemistry. *J. Phys. Chem. C* **2009**, *113*, 6327–6359.
5. Tachikawa, T.; Fujitsuka, M.; Majima, T. Mechanistic Insight into the TiO_2 Photocatalytic Reactions: Design of New Photocatalysts. *J. Phys. Chem. C* **2007**, *111*, 5259–5275.
6. Kim, D.; Ghicov, A.; Albu, S. P.; Schmuki, P. Bamboo-Type TiO_2 Nanotubes: Improved Conversion Efficiency in Dye-Sensitized Solar Cells. *J. Am. Chem. Soc.* **2008**, *130*, 16454–16455.
7. Baker, D. R.; Kamat, P. V. Photosensitization of TiO_2 Nanostructures with CdS Quantum Dots. Particulate *versus* Tubular Support Architectures. *Adv. Funct. Mater.* **2009**, *19*, 805–811.
8. Zhu, K.; Neale, N. R.; Miedaner, A.; Frank, A. J. Enhanced Charge-Collection Efficiencies and Light Scattering in Dye-Sensitized Solar Cells Using Oriented TiO_2 Nanotubes Arrays. *Nano Lett.* **2007**, *7*, 69–74.
9. Kongkanand, A.; Tvrdy, K.; Takechi, K.; Kuno, M. K.; Kamat, P. V. Quantum Dot Solar Cells. Tuning Photoresponse through Size and Shape Control of CdSe−TiO_2 Architecture. *J. Am. Chem. Soc.* **2008**, *130*, 4007–4015.
10. Mor, G. K.; Shankar, K.; Paulose, M.; Varghese, O. K.; Grimes, C. A. Use of Highly-Ordered TiO_2 Nanotube Arrays in Dye-Sensitized Solar Cells. *Nano Lett.* **2006**, *6*, 215–218.
11. Jennings, J. R.; Ghicov, A.; Peter, L. M.; Schmuki, P.; Walker, A. B. Dye-Sensitized Solar Cells Based on Oriented TiO_2 Nanotube Arrays: Transport, Trapping, and Transfer of Electrons. *J. Am. Chem. Soc.* **2008**, *130*, 13364–13372.
12. Roy, P.; Kim, D.; Paramasivam, I.; Schmuki, P. Improved Efficiency of TiO_2 Nanotubes in Dye Sensitized Solar Cells by Decoration with TiO_2 Nanoparticles. *Electrochem. Commun.* **2009**, *11*, 1001–1004.
13. Mohapatra, S. K.; Misra, M. Enhanced Photoelectrochemical Generation of Hydrogen from Water by 2,6-Dihydroxyantraquinone-Functionalized Titanium Dioxide Nanotubes. *J. Phys. Chem. C* **2007**, *111*, 11506–11510.
14. Mohapatra, S. K.; Misra, M.; Mahajan, V. K.; Raja, K. S. Design of a Highly Efficient Photoelectrolytic Cell for Hydrogen Generation by Water Splitting: Application of $TiO_{2-x}C_x$ Nanotubes as a Photoanode and Pt/TiO_2 Nanotubes as a Cathode. *J. Phys. Chem. C* **2007**, *111*, 8677–8685.
15. Ruan, C. M.; Paulose, M.; Varghese, O. K.; Grimes, C. A. Enhanced Photo Electrochemical-Response in Highly Ordered TiO_2 Nanotube-Arrays Anodized in Boric Acid Containing Electrolyte. *Sol. Energy Mater. Sol. Cells* **2006**, *90*, 1283–1295.
16. Mor, G. K.; Shankar, K.; Paulose, M.; Varghese, O. K.; Grimes, C. A. Enhanced Photocleavage of Water Using Titania Nanotube Arrays. *Nano Lett.* **2005**, *5*, 191–195.
17. Wang, Q.; Zhu, K.; Neale, N. R.; Frank, A. J. Constructing Ordered Sensitized Heterojunctions: Bottom-Up Electrochemical Synthesis of p-Type Semiconductors in Oriented *n*-TiO_2 Nanotube Arrays. *Nano Lett.* **2009**, *9*, 806–813.
18. Adachi, M.; Murata, Y.; Okada, I.; Yoshikawa, S. Formation of Titania Nanotubes and Applications for Dye-Sensitized Solar Cells. *J. Electrochem. Soc.* **2003**, *150*, G488–G493.
19. Kongkanand, A.; Domínguez, R. M.; Kamat, P. V. Single Wall Carbon Nanotube Scaffolds for Photoelectrochemical Solar Cells. Capture and Transport of Photogenerated Electrons. *Nano Lett.* **2007**, *7*, 676–680.
20. Vietmeyer, F.; Seger, B.; Kamat, P. V. Anchoring ZnO Particles on Functionalized Single Wall Carbon Nanotubes. Excited State Interactions and Charge Collection. *Adv. Mater.* **2007**, *19*, 2935–2940.
21. Hasobe, T.; Fukuzumi, S.; Kamat, P. V. Organized Assemblies of Single Wall Carbon Nanotubes and Porphyrin for Photochemical Solar Cells: Charge Injection from Excited Porphyrin into Single-Walled Carbon Nanotubes. *J. Phys. Chem. B* **2006**, *110*, 25477–25484.
22. Martinson, A. B. F.; Elam, J. W.; Hupp, J. T.; Pellin, M. J. ZnO Nanotube Based Dye-Sensitized Solar Cells. *Nano Lett.* **2007**, *7*, 2183–2187.
23. Brown, P. R.; Takechi, K.; Kamat, P. V. Single-Walled Carbon Nanotube Scaffolds for Dye-Sensitized Solar Cells. *J. Phys. Chem. C* **2008**, *112*, 4776–4782.
24. Fabregat-Santiago, F.; Barea, E. M.; Bisquert, J.; Mor, G. K.; Shankar, K.; Grimes, C. A. High Carrier Density and Capacitance in TiO_2 Nanotube Arrays Induced by Electrochemical Doping. *J. Am. Chem. Soc.* **2008**, *130*, 11312–11316.
25. Seabold, J. A.; Shankar, K.; Wilke, R. H. T.; Paulose, M.; Varghese, O. K.; Grimes, C. A.; Choi, K. S. Photoelectrochemical Properties of Heterojunction CdTe/TiO_2 Electrodes Constructed Using Highly Ordered TiO_2 Nanotube Arrays. *Chem. Mater.* **2008**, *20*, 5266–5273.
26. Chen, X.; Mao, S. S. Titanium Dioxide Nanomaterials: Synthesis, Properties, Modifications, and Applications. *Chem. Rev.* **2007**, *107*, 2891–2959.
27. Fujishima, A.; Honda, K. Electrochemical Photolysis of Water at a Semiconductor Electrode. *Nature* **1972**, *238*, 37–38.

28. Gerischer, H.; Luebke, M. A Particle Size Effect in the Sensitization of TiO_2 Electrodes by a CdS Deposit. *J. Electroanal. Chem.* **1986**, *204*, 225–227.
29. Willner, I.; Eichen, Y. TiO_2 and CdS Colloids Stabilized by Beta-Cyclodextrins: Tailored Semiconductor−Receptor Systems as a Means to Control Interfacial Electron-Transfer Processes. *J. Am. Chem. Soc.* **1987**, *109*, 6862–6863.
30. Gopidas, K. R.; Bohorquez, M.; Kamat, P. V. Photoelectrochemistry in Semiconductor Particulate Systems. 16. Photophysical and Photochemical Aspects of Coupled Semiconductors. Charge-Transfer Processes in Colloidal CdS−TiO_2 and CdS−AgI Systems. *J. Phys. Chem.* **1990**, *94*, 6435–6440.
31. Kohtani, S.; Kudo, A.; Sakata, T. Spectral Sensitization of a TiO_2 Semiconductor Electrode by CdS Microcrystals and its Photoelectrochemical Properties. *Chem. Phys. Lett.* **1993**, *206*, 166–170.
32. Vinodgopal, K.; Bedja, I.; Kamat, P. V. Nanostructured Semiconductor Films for Photocatalysis. Photoelectrochemical Behavior of SnO_2/TiO_2 Coupled Systems and Its Role in Photocatalytic Degradation of a Textile Azo Dye. *Chem. Mater.* **1996**, *8*, 2180–2187.
33. Bedja, I.; Kamat, P. V. Capped Semiconductor Colloids. Synthesis and Photoelectrochemical Properties of TiO_2 Capped SnO_2 Surfaces. *J. Phys. Chem.* **1995**, *99*, 9182–9188.
34. Sant, P. A.; Kamat, P. V. Inter-Particle Electron Transfer between Size-Quantized CdS and TiO_2 Semiconductor Nanoclusters. *Phys. Chem. Chem. Phys.* **2002**, *4*, 198–203.
35. Rajeshwar, K.; de Tacconi, N. R.; Chenthamarakshan, C. R. Semiconductor-Based Composite Materials: Preparation, Properties, and Performance. *Chem. Mater.* **2001**, *13*, 2765–2782.
36. Niitsoo, O.; Sarkar, S. K.; Pejoux, C.; Ruhle, S.; Cahen, D.; Hodes, G. Chemical Bath Deposited CdS/CdSe-Sensitized Porous TiO_2 Solar Cells. *J. Photochem. Photobiol. A* **2006**, *181*, 306–313.
37. Bang, J. H.; Kamat, P. V. Quantum Dot Sensitized Solar Cells. A Tale of Two Semiconductor Nanocrystals: CdSe and CdTe. *ACS Nano* **2009**, *3*, 1467–1476.
38. Harris, C. T.; Kamat, P. V. Photocatalysis with CdSe Nanoparticles in Confined Media: Mapping Charge Transfer Events in the Subpicosecond to Second Timescales. *ACS Nano* **2009**, *3*, 682–690.
39. Asahi, R.; Morikawa, T.; Ohwaki, T.; Aoki, K.; Taga, Y. Visible-Light Photocatalysis in Nitrogen-Doped Titanium Oxides. *Science* **2001**, *293*, 269–271.
40. Khan, S. U. M.; Al-Shahry, M.; Ingler, W. B., Jr. Efficient Photochemical Water Splitting by a Chemically Modified *n*-TiO_2. *Science* **2002**, *297*, 2243–2245.
41. Ghicov, A.; Macak, J. M.; Tsuchiya, H.; Kunze, J.; Haeublein, V.; Frey, L.; Schmuki, P. Ion Implantation and Annealing for an Efficient N-Doping of TiO_2 Nanotubes. *Nano Lett.* **2006**, *6*, 1080–1082.
42. Vitiello, R. P.; Macak, J. M.; Ghicov, A.; Tsuchiya, H.; Dick, L. F. P.; Schmuki, P. N-Doping of Anodic TiO_2 Nanotubes Using Heat Treatment in Ammonia. *Electrochem. Commun.* **2006**, *8*, 544–548.
43. Hahn, R.; Schmidt-Stein, F.; Salonen, J.; Thiemann, S.; Song, Y. Y.; Kunze, J.; Lehto, V. P.; Schmuki, P. Semimetallic TiO_2 Nanotubes. *Angew. Chem., Int. Ed.* **2009**, *48*, 7236–7239.
44. Diamant, Y.; Chen, S. G.; Melamed, O.; Zaban, A. Core−Shell Nanoporous Electrode for Dye Sensitized Solar Cells: The Effect of the $SrTiO_3$ Shell on the Electronic Properties of the TiO_2 Core. *J. Phys. Chem. B* **2003**, *107*, 1977–1981.
45. Tsumura, T.; Sogabe, K.; Toyoda, M. Preparation of $SrTiO_3$-Supported TiO_2 Photocatalyst. *Mater. Sci. Eng., B* **2009**, *157*, 113–115.
46. Li, Y.; Gao, X. P.; Li, G. R.; Pan, G. L.; Yan, T. Y.; Zhu, H. Y. Titanate Nanofiber Reactivity: Fabrication of $MTiO_3$ (M = Ca, Sr, and Ba) Perovskite Oxides. *J. Phys. Chem. C* **2009**, *113*, 4386–4394.
47. Schaak, R. E.; Mallouk, T. E. Topochemical Synthesis of Three-Dimensional Perovskites from Lamellar Precursors. *J. Am. Chem. Soc.* **2000**, *122*, 2798–2803.
48. Iwata, N.; Yamaguchi, K.; Nishimura, T. B.; Takemura, K.; Miyasaka, Y. Li-Ion Battery Operated Power Amplifier MMICs Utilizing $SrTiO_3$ Capacitors and Heterojunction FETs for PDC and CDMA Cellular Phones. *Solid-State Electron.* **1999**, *43*, 747–753.
49. Miyauchi, M.; Takashio, M.; Tobimatsu, H. Photocatalytic Activity of $SrTiO_3$ Codoped with Nitrogen and Lanthanum Under Visible Light Illumination. *Langmuir* **2004**, *20*, 232–236.
50. Kato, H.; Kudo, A. Visible-Light-Response and Photocatalytic Activities of TiO_2 and $SrTiO_3$ Photocatalysts Codoped with Antimony and Chromium. *J. Phys. Chem. B* **2002**, *106*, 5029–5034.
51. Choi, J. Y.; Kim, C. H.; Kim, D. K. Hydrothermal Synthesis of Spherical Perovskite Oxide Powders Using Spherical Gel Powders. *J. Am. Ceram. Soc.* **1998**, *81*, 1353–1356.
52. Wrighton, M. S.; Ellis, A. B.; Wolczanski, P. T.; Morse, D. L.; Abrahamson, H. B.; Ginley, D. S. Strontium Titanate Photoelectrodes. Efficient Photoassisted Electrolysis of Water at Zero Applied Potential. *J. Am. Chem. Soc.* **1976**, *98*, 2774–2779.
53. Hwang, Y. J.; Boukai, A.; Yang, P. D. High Density *n*-Si/*n*-TiO_2 Core/Shell Nanowire Arrays with Enhanced Photoactivity. *Nano Lett.* **2009**, *9*, 410–415.
54. Lin, Y. J.; Zhou, S.; Liu, X. H.; Sheehan, S.; Wang, D. W. TiO_2/$TiSi_2$ Heterostructures for High-Efficiency Photoelectrochemical H_2O Splitting. *J. Am. Chem. Soc.* **2009**, *131*, 2772–2773.
55. Zwilling, V.; Darque-Ceretti, E.; Boutry-Forveille, A.; David, D.; Perrin, M. Y.; Aucouturier, M. Structure and Physicochemistry of Anodic Oxide Films on Titanium and TA6V Alloy. *Surf. Interface Anal.* **1999**, *27*, 629–637.
56. Gong, D.; Grimes, C. A.; Varghese, O. K.; Hu, W. C.; Singh, R. S.; Chen, Z.; Dickey, E. C. Titanium Oxide Nanotube Arrays Prepared by Anodic Oxidation. *J. Mater. Res.* **2001**, *16*, 3331–3334.
57. Varghese, O. K.; Gong, D.; Paulose, M.; Ong, K. G.; Dickey, E. C.; Grimes, C. A. Extreme Changes in the Electrical Resistance of Titania Nanotubes with Hydrogen Exposure. *Adv. Mater.* **2003**, *15*, 624–627.
58. Ruan, C.; Paulose, M.; Varghese, O. K.; Mor, G. K.; Grimes, C. A. Fabrication of Highly Ordered TiO_2 Nanotube Arrays Using an Organic Electrolyte. *J. Phys. Chem. B* **2005**, *109*, 15754–15759.
59. Macak, J. M.; Sirotna, K.; Schmuki, P. Self-Organized Porous Titanium Oxide Prepared in Na_2SO_4/NaF Electrolytes. *Electrochim. Acta* **2005**, *50*, 3679–3684.
60. Macak, J. M.; Tsuchiya, H.; Schmuki, P. High-Aspect-Ratio TiO_2 Nanotubes by Anodization of Titanium. *Angew. Chem., Int. Ed.* **2005**, *44*, 2100–2102.
61. Zhu, K.; Vinzant, T. B.; Neale, N. R.; Frank, A. J. Removing Structural Disorder from Oriented TiO_2 Nanotube Arrays: Reducing the Dimensionality of Transport and Recombination in Dye-Sensitized Solar Cells. *Nano Lett.* **2007**, *7*, 3739–3746.
62. Varghese, O. K.; Gong, D. W.; Paulose, M.; Grimes, C. A.; Dickey, E. C. Crystallization and High-Temperature Structural Stability of Titanium Oxide Nanotube Arrays. *J. Mater. Res.* **2003**, *18*, 156–165.
63. Wang, Y.; Xu, H.; Wang, X.; Zhang, X.; Jia, H.; Zhang, L.; Qiu, J. A General Approach to Porous Crystalline TiO_2, $SrTiO_3$, and $BaTiO_3$ Spheres. *J. Phys. Chem. B* **2006**, *110*, 13835–13840.
64. Jitputti, J.; Charoensirithavorn, P.; Yoshikawa, S. Hydrothermal Production of $SrTiO_3$ Nanotube Arrays. *Chem. Lett.* **2007**, *36*, 1508–1509.
65. Xin, Y.; Jiang, J.; Huo, K.; Hu, T.; Chu, P. K. Bioactive $SrTiO_3$ Nanotube Arrays: Strontium Delivery Platform on Ti-Based Osteoporotic Bone Implants. *ACS Nano* **2009**, *3*, 3228–3234.
66. Zhao, J.; Wang, X.; Chen, R.; Li, L. Synthesis of Thin Films of Barium Titanate and Barium Strontium Titanate Nanotubes on Titanium Substrates. *Mater. Lett.* **2005**, *59*, 2329–2332.

67. Wei, X.; Vasiliev, A. L.; Padture, N. P. Nanotubes Patterned Thin Films of Barium−Strontium Titanate. *J. Mater. Res.* **2005**, *20*, 2140–2147.
68. Hodes, G.; Howell, I. D. J.; Peter, L. M. Nanocrystalline Photoelectrochemical Cells. A New Concept in Photovoltaic Cells. *J. Electrochem. Soc.* **1992**, *139*, 3136–3140.
69. Vinodgopal, K.; Hotchandani, S.; Kamat, P. V. Electrochemically Assisted Photocatalysis. TiO_2 Particulate Film Electrodes for Photocatalytic Degradation of 4-Chlorophenol. *J. Phys. Chem.* **1993**, *97*, 9040–9044.
70. Subramanian, V.; Wolf, E. E.; Kamat, P. V. Catalysis with TiO_2/Au Nanocomposites. Effect of Metal Particle Size on the Fermi Level Equilibration. *J. Am. Chem. Soc.* **2004**, *126*, 4943–4950.
71. Diamant, Y.; Chappel, S.; Chen, S. G.; Melamed, O.; Zaban, A. Core−Shell Nanoporous Electrode for Dye Sensitized Solar Cells: The Effect of Shell Characteristics on The Electronic Properties of The Electrode. *Coord. Chem. Rev.* **2004**, *248*, 1271–1276.
72. Burnside, S.; Moser, J. E.; Brooks, K.; Graetzel, M.; Cahen, D. Nanocrystalline Mesoporous Strontium Titanate as Photoelectrode Material for Photosensitized Solar Devices: Increasing Photovoltage through Flatband Potential Engineering. *J. Phys. Chem. B* **1999**, *103*, 9328–9332.
73. Bolts, J. M.; Wrighton, M. S. Correlation of Photocurrent−Voltage Curves with Flat-Band Potential for Stable Photoelectrodes for Photoelectrolysis of Water. *J. Phys. Chem.* **1976**, *80*, 2641–2645.